ELSEVIER

https://www.jhltopen.org/

Pediatric continuous-flow total artificial heart with rotor axial position tracking technology: First report of in vivo assessment

Chihiro Miyagi, MD, PhD,[a] Taiyo Kuroda, MD,[a] Anthony R. Polakowski, BS, MEng,[a] Christine R. Flick, BS,[a] Shengqiang Gao, PhD,[a] Barry D. Kuban, BS,[a] Jamshid H. Karimov, MD, PhD,[a,b,c,*] and Kiyotaka Fukamachi, MD, PhD[a,b,c]

[a]*Department of Biomedical Engineering, Lerner Research Institute, Cleveland Clinic, Cleveland, Ohio*
[b]*Cleveland Clinic Lerner College of Medicine of Case Western Reserve University, Cleveland, Ohio*
[c]*Kaufman Center for Heart Failure, Heart, Vascular, and Thoracic Institute, Cleveland, Ohio*

KEYWORDS:
pediatric heart failure;
congenital heart disease;
mechanical circulatory support;
pediatric total artificial heart;
large animal study

BACKGROUND: The pediatric continuous-flow total artificial heart (P-CFTAH) is a novel double-ended centrifugal pump designed with the intent to provide circulatory support for pediatric heart failure. To enable continuous monitoring of pump hemodynamics, Hall effect sensors (HES) were embedded inside the P-CFTAH design to track both axial movement and position of the pump rotor post-implantation. Herein, we report an early in vivo evaluation of the P-CFTAH with HES, implanted in small-sized ovine models.

METHODS: Five healthy lambs were used for the P-CFTAH implantation via a full median sternotomy and cardiopulmonary bypass support. Successful evaluation of the P-CFTAH was achieved in 4 out of 5 (n = 4, 20.9 ± 1.3 kg). The hemodynamics and operating conditions were continuously recorded with varying pump speeds (2,800-5,000 rpm), systemic/pulmonary vascular resistance ratio, and high- and low-volume conditions. Among the 4 cases, P-CFTAH with HES embedded in the rotor was used in 2 cases.

RESULTS: All surgical procedures were uneventful, and the optimal anatomical fit of the pump was shown in the chest. Differences between the left and right atrial pressures were mostly maintained within the intended limit of ± 10 mm Hg throughout the design range of systemic and pulmonary vascular resistance. The HES accurately traced the rotor position, showing a positive correlation with atrial pressure differences.

CONCLUSIONS: The findings suggest that the P-CFTAH has the potential to provide self-balancing circulatory support for pediatric heart failure patients. The study contributes to the development of a pediatric-sized total artificial heart with improved monitoring.

JHLT Open 2024;5:100118

*Corresponding author: Jamshid H. Karimov, MD, PhD, Department of Biomedical Engineering/ND20, Lerner Research Institute, Cleveland Clinic, 9500 Euclid Avenue, Cleveland, OH 44195.
E-mail address: karimoj.cc@gmail.com.

https://doi.org/10.1016/j.jhlto.2024.100118

Background

In the last 3 decades, there have been significant changes in the environment that surrounds pediatric heart failure patients requiring mechanical circulatory support devices and subsequent heart transplantation. The annual pediatric heart transplant report of the International Thoracic Organ Transplant Registry published in 2020, 2021, and 2022 focused on the evolving changes between each decade in respective categories: donor characteristics,[1] recipient characteristics,[2] and infant heart transplantation.[3] When examining the recipient characteristics, the percentage of recipients supported by a mechanical circulatory support device from 2010 to 2018 (25.7%) nearly doubled when compared to the previous decade during (13.7% from 2001-2009). Among the recipients, biventricular support via biventricular assist device (BiVAD) or total artificial heart (TAH) also exhibited a definitive increase from 3.9% to 5.7%. While the ventricular assist device, as a representative of the mechanical circulatory support, has yielded better outcomes in pediatric heart failure population,[4-7] advanced-stage pediatric heart failure patients might have potentially benefited more from a replacement therapy, such as TAH. This is further evinced when considering the presence of bilateral heart failure in single ventricular patients, patients' limited chest space, and/or possibility of chronic rejection/infection after transplantation.[8-11]

The only current option for a pediatric TAH device, however, is seriously limited to the SynCardia 50 cc (SynCardia Systems, LLC, Tucson, AZ), and the recommended patient size for the 50 cc pump requires a body surface area of 1.2 to 1.7 m^2.[10-12] To address this critical clinical need, our group has been investigating the pediatric continuous-flow TAH (P-CFTAH), a TAH we have developed through scaling down the adult continuous-flow TAH (CFTAH), for even further, smaller-size patients (e.g., minimum body surface area of target population: 0.3 m^2). Initial in vivo experimental results in ovine models around 30 kg have been previously reported.[13] The advanced design has been further refined, now enabling the incorporation of miniature Hall effect sensors (HES) into the P-CFTAH architecture to continuously monitor the axial movement and position of the pump rotor. The aim of this study is to investigate in more detail the P-CFTAH function with embedded HES in smaller-sized ovine animal models.

Material and methods

Device description

The P-CFTAH creates self-balancing left and right circulations with 4 major assembly subcomponents: right housing (Figure 1A); stator assembly (Figure 1B); left housing (Figure 1C); and rotating assembly (Figure 1D-F). With a double-ended centrifugal pump concept, the only moving part is the rotor assembly; self-balancing was achieved without electronic intervention.[14-16] The pump size is 4.3 cm in diameter, 7.0 cm in body length, and 13 ml as a priming volume (Figure 1G and H). Originally, the pump was made by scaling down the adult CFTAH with the same algorithm and with a scale factor of 0.70.

A novel, customized proprietary motor control system (Figure S1A) based on hardware from NXP Semiconductors (Austin, TX) was built. Additionally, a control method called field-oriented control was used, which produces the maximum motor torque with minimal wasted power. A unique feature of this control method is that it separates the 2 components of the magnetic force that drives the motor: the direct force that acts in the radial direction, and the quadrature force that acts in the tangential direction. As the direct force does not contribute to the motor rotation, the control system is continuously adjusting the motor-winding currents, in an effort to both minimize the power to the direct force and maximize the power used for the quadrature force. This results in a highly power-efficient system that extracts the maximum amount of torque from a given motor. Using the most efficient control system allows for the use of the smallest motor possible to achieve the pump requirements, which is essential to minimize the ultimate size and weight of implantable devices.

As for the controller interface, our team has developed novel, proprietary firmware for the controller board, an addition to custom user-interface software (Figure S1B) that enables simple control and monitoring of the pump. This interface software allows the user to choose the mean speed of the pump; although the P-CFTAH pump is a continuous-flow pump, pulsatile flow can be fine-tuned by modulating the speed of the pump at a chosen heart rate and pulse amplitude.

Thus far, initial evaluations have consisted of an in vitro study,[17] 4 in vivo experiments using lambs around 30 kg,[13] and human fitting studies conducted both intraoperatively and digitally on a computer, using 3-dimensional (3D) computed tomography images.[18] After several interactions of the design, guided by the necessary updates primarily derived from computed fluid dynamics simulations, a next-generation, evolved "working" prototype of the P-CFTAH was fabricated, comprising a 3D-printed rotating assembly and titanium housing.

Hall effect sensors

The stator assembly of the P-CFTAH is instrumented with HES at both ends to monitor the axial movement of the rotating assembly, the same design as that of the adult CFTAH used during in vitro testing.[14] A more detailed description of HES components is separately included with the Supplemental Material.

In vivo study

The study protocol was approved by Cleveland Clinic's Institutional Animal Care and Use Committee (#00001876). For this study, a total of 5 acute in vivo studies were performed, which used Dorset lambs under general anesthesia and cardiopulmonary bypass support. The P-CFTAH was

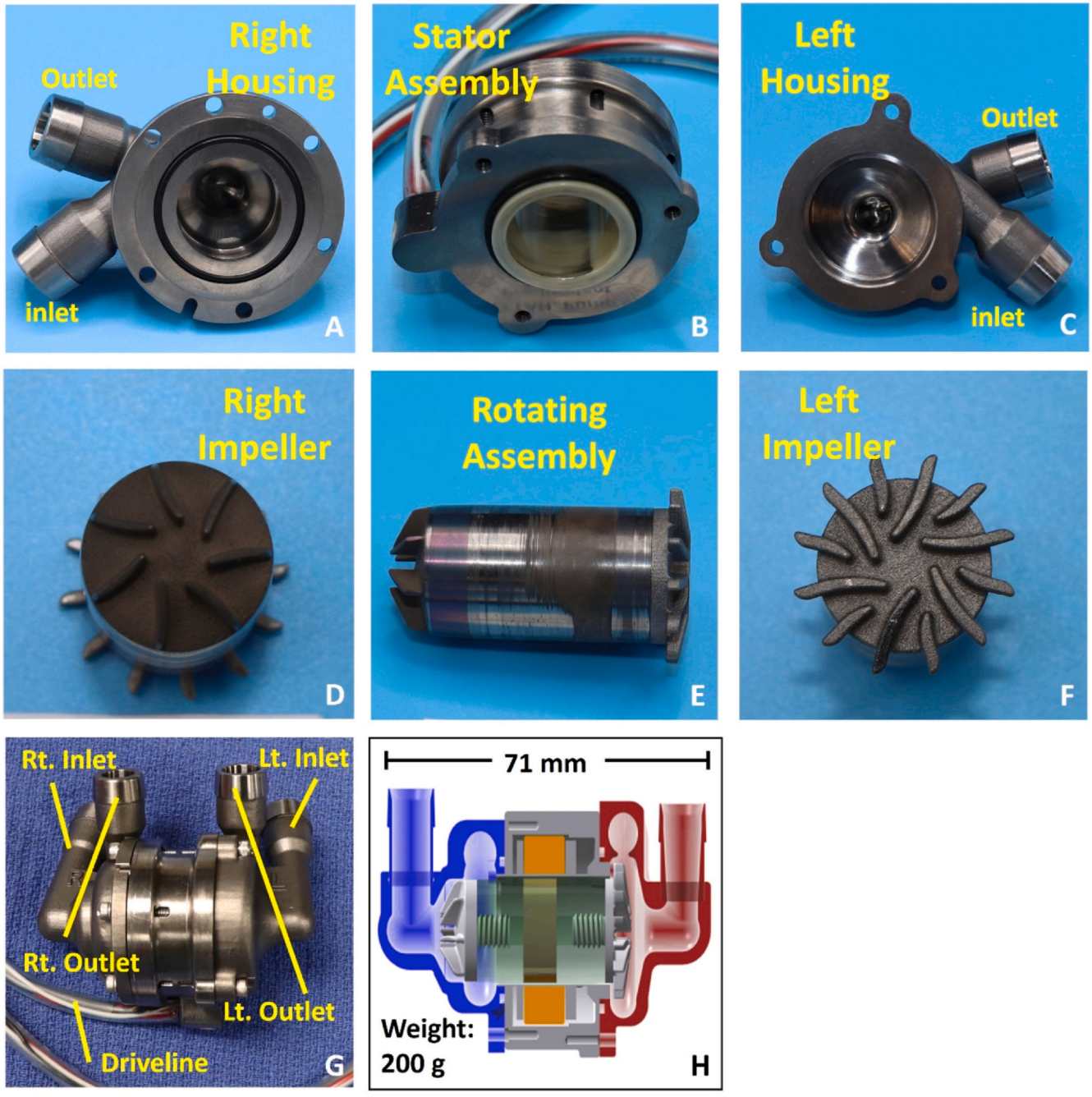

Figure 1 Exploded view of P-CFTAH pump showing the 4 major assembly subcomponents: (A) right housing, (B) stator assembly, (C) left pump housing, (D) right impeller of rotor assembly, (E) rotor assembly, and (F) lift impeller of rotor assembly. (G) Photo of assembled P-CFTAH and (H) a schematic illustration of assembled P-CFTAH. P-CFTAH, pediatric continuous-flow total artificial heart.

successfully implanted in 4 of the 5 cases (mean body weight: 20.9 ± 1.3 kg) via median sternotomy. In the sole remaining case, the pump failed to operate due to a non-concentric rotor that made the controller feedback unstable; thus, the case was terminated.

Surgical procedures for the in vivo studies were the same as in the previous report.[13] Cardiopulmonary bypass was established under full heparinization (300 U/kg). After cross-clamping the ascending aorta and main pulmonary artery (PA), both ventricles were resected at the atrioventricular groove and roots of the aorta and the PA (Figure 2A). Inflow cuffs were sutured to the atria over Teflon strips (BARD PTFE Felt, 007976, Bard Peripheral Vascular, Inc., Tempe, AZ) (Figure 2B) and outflow grafts were anastomosed to the aorta and the PA (Figure 2C and D) with running sutures. Both pump chambers of the P-CFTAH were primed with saline and connected to the inflow cuffs and outflow conduits. After deairing the atria and pump, the P-CFTAH was gradually started, and cardiopulmonary bypass was weaned. Pump performance and hemodynamic stability were recorded and evaluated at predetermined varying speed settings, and induced hemodynamic states are described in more detail below.

After induction of each specified state and subsequent recording of all hemodynamic data, Beuthanasia (100 mg/

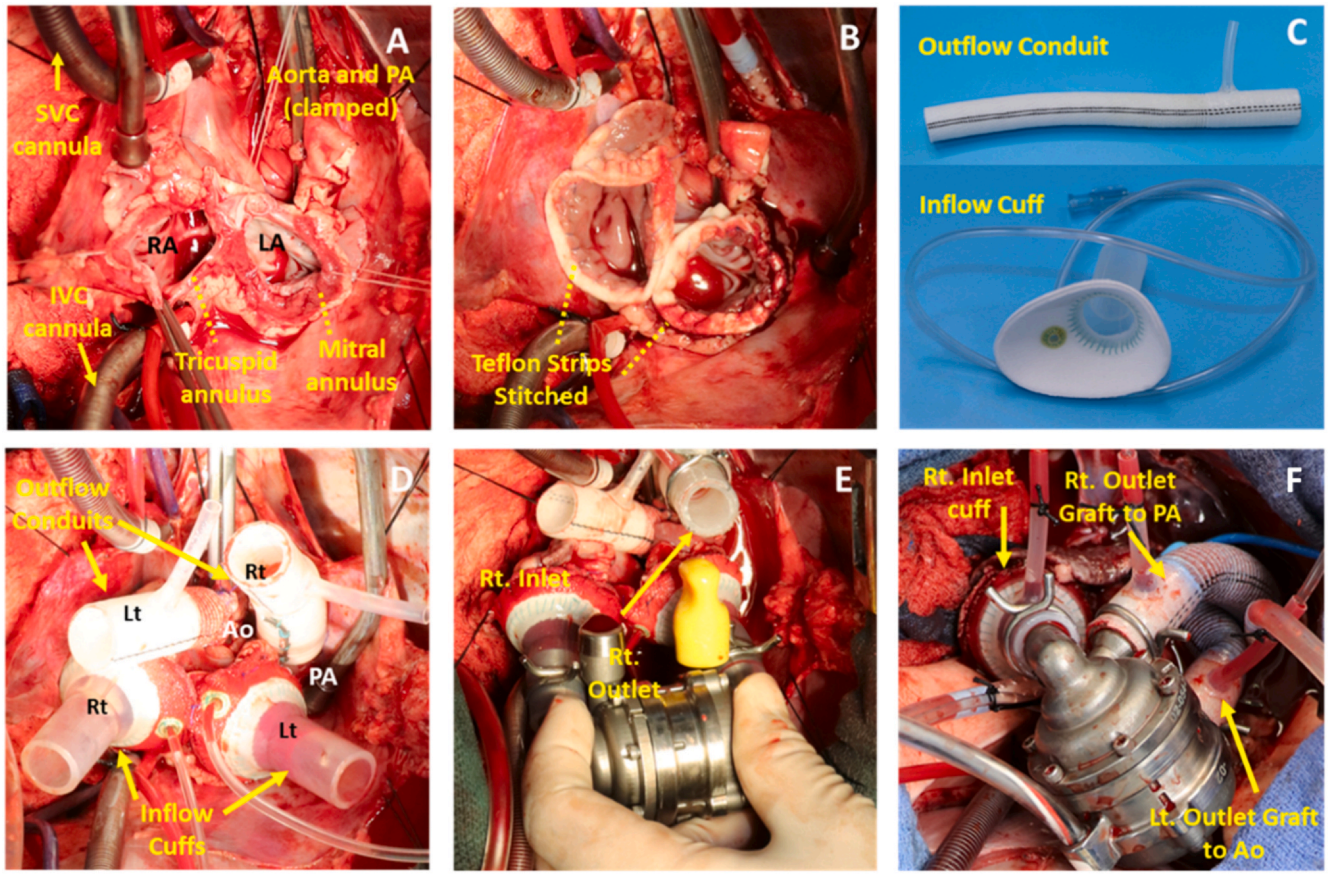

Figure 2 Intraoperative photos of the P-CFTAH implantation in a lamb. Ao, aorta; IVC, inferior vena cava; PA, pulmonary artery; P-CFTAH, pediatric continuous-flow total artificial heart; SVC, superior vena cava.

kg) was administered, and the P-CFTAH pump was stopped under 5% isoflurane. In every case, the pump was inspected after the termination of the study, adhering to the standard procedure.

Hemodynamic analysis of pump performance

The following parameters were continuously monitored while the chest remained open: (1) right and left atrial pressures (RAP and LAP); (2) systemic arterial pressure, pulmonary arterial pressure, and central venous pressure; (3) total systemic blood flow via a 14 mm or 16 mm flow probe (Transonic Systems Inc., Ithaca, NY) placed at either the native ascending aorta or around the right outflow graft; and (4) pump speed and motor current from the P-CFTAH controller.

Changes in pump settings (i.e., speed (3,000-5,000 rpm), speed modulation (80-120 bpm), and pulsatility (0%-25%), etc.) were generated, and the hemodynamics at each of the steady states were recorded. High and low blood-volume statuses were also implemented by fluid volume adjustment. Additionally, a wide range of systemic and pulmonary vascular resistance (SVR and PVR, respectively) ratios were induced through different levels of partial occlusion of the outflow grafts of either or both sides and/or by vasodilator (nitroprusside or isoflurane). SVR and PVR were calculated and recorded as:

$$SVR = (\text{aortic pressure} - RAP) \times 80/(\text{pump flow})$$

$$PVR = (\text{Pulmonary arterial pressure} - LAP) \times 80/(\text{pump flow})$$

Hemodynamics and pump performance parameters were digitized at a sampling rate of 200 Hz using the PowerLab data acquisition system (ADInstruments, Inc., Colorado Springs, CO), analyzed with LabChart (ADInstruments), and then downloaded into a Microsoft Excel file (Microsoft, Redmond, WA), summarizing and charting test results.

The following states of hemodynamics were induced and recorded in all 4 cases after the state of baseline (at 3,500 rpm, 80 bpm, 10% of pulsatility): (1) speed change (from 3,000-5,000 rpm); (2) speed modulation change (80, 100, and 120 bpm); (3) pulsatility change (amplitude of speed modulation: 0%, 10%, 15%, and 25%); (4) high SVR; (5) high PVR; (6) high SVR + high PVR; (7) high SVR and low PVR; (8) low SVR and high PVR; (9) low SVR and low PVR; (10) low circulating blood volume (target central venous pressure = 0-2 mm Hg); and (11) high circulating blood volume (target central venous pressure > 10 mm Hg). The order of the aforementioned states, especially with regard to states 6 through 9 in our list, varied depending on each experiment. However, in each setting, the hemodynamics were recorded upon achieving a stable state free from the influences of previous states.

In the most recent 2 cases, rotor response in its axial position toward the pressure change of the pump inlet was measured and recorded by the HES, and mean rotor positions at each condition were recorded as a distance from the neutral position (mm) in a stable state. Of note, HES in the P-CFTAH were used only for tracking and monitoring the rotor behavior; therefore, exhibiting neither influence nor interference on the pump control.

Statistical analysis

Data are presented as mean values, and the correlations between the rotor position (V) and atrial pressure differences (LAP – RAP, mm Hg) were assessed, using Spearman's Rank correlation coefficient. A value where $p < 0.05$ was considered statistically significant. Statistical analyses were performed using the JMP Pro 14.2.0 Statistical Discovery Software (SAS Institute Inc., Cary, NC).

Results

In the study's 4 cases where the P-CFTAH was successfully implanted, the pump exhibited an acceptable anatomical fit, and the implantation procedures were uneventful. After adjustments of the volume status for sheep, the resultant flow created by the P-CFTAH pump was adequately maintained, and the baseline hemodynamics were kept stable. With regards to all control inputs, the pump responded as intended, demonstrating stable device performance without any power elevations and/or mechanical failures.

Table 1 shows mean hemodynamic parameters at baseline, and 11 pump settings of the 4 cases: (1) speed change from 3,500 to 5,000 rpm; (2) beat rate change at 80, 100, and 120 bpm; (3) pulse index change at 0%, 10%, 15%, and 25%; (4) high SVR; (5) high PVR; (6) high SVR and high PVR; (7) high SVR and low PVR; (8) low SVR and high PVR; (9) low SVR and low PVR; (10) high volume; and (11) low volume. Utilizing data from one of the cases, Figure 3 illustrates a representative time chart of the main parameters. Between the settings of measurements 4 through 8, several different extents of partial occlusion of the aorta and/or the PA were tried, 1 to 3 times each. At the various high-volume settings (list item 10), 6 speed settings (2,800, 3,000, 3,500, 4,000, 4,500, and 5,000 rpm for this case) were tried. For the low-volume settings, gradual volume reduction for 3 points were tested at 2,800 rpm, and the last point was taken at 2,500 rpm.

Figure 4 depicts the plots of the mean rotor position, at each delta pressure (atrial pressure difference between left atrium (LA) and right atrium (RA)) from the last 2 series with the HES. This shows a clear positive correlation ($R = 0.937$, $p < 0.01$), and, thus, indicates that (1) the rotor position exhibited a good response, depending on the atrial pressure differences, and (2) the HES reliably tracked position of the rotor. Throughout these 2 cases, the axial position of the rotor obtained by the HES, followed well along with the delta pressure of each atrium. To show this in more detail, a time chart from one of the cases, illustrating the delta pressure of both the atria and the rotor position throughout the entire experiment is displayed in Figure 5.

As for self-regulating performance of the P-CFTAH, the differences between LAP and RAP remained ± 10 mm Hg for most of the plotting points, demarcating the various SVR and PVR settings within design range (120 of the 147 points with SVR/PVR = 1.0-15.0) (Figure 6).

Discussion

Throughout this study's in vivo series, our team has demonstrated reasonable self-regulation of the P-CFTAH, at various test configurations, as well as the satisfactory response of HES-derived axial rotor position tracking under all test conditions. Notably, the implantation of the pump in small lambs that weigh around 20 kg represented the first attempt using this pump.

In populations with congenital heart disease (CHD), patients often experience heart failure in both ventricles and require biventricular support. Currently, 13% of patients are supported with a BiVAD according to the Sixth Annual Pedimacs report.[19] However, when looking at the overall usage of BiVAD support, there has been a notable decline in the frequency of BiVAD usage over the past decade. This can be primarily attributed to the Berlin Heart EXCOR Pediatric Investigational Device Exemption study, which ultimately indicated that BiVAD support was a predictor of early mortality.[20] For smaller children particularly, the limited space within the chest cavity presents a challenging environment to accommodate 2 ventricular assist devices, and subsequently, effectively balancing the 2 pumps tends to be problematic. Especially within this context, our group's P-CFTAH offers a novel, valuable solution. It can manage both systemic and pulmonary circulations with a single pump, while automatically and passively adjusting both flows based on the preload balance of the left and right circulations.

Another benefit of the P-CFTAH's self-balancing concept in patients with CHD is its ability to address flow discrepancies between the left and right circulations, a common occurrence in CHD patients, mainly attributed to bronchial shunts. The shunt flow constitutes up to one-third of the systemic output in patients requiring a TAH[21]; thus, shunt flow should not be ignored whenever a TAH implantation is considered.

When evaluating the self-balancing feature of the CFTAH-type devices, our research team has frequently used HES for both in vitro and in vivo studies.[14] In the P-CFTAH pump, HES successfully detected and visualized the position of the rotor assembly, thereby enabling the

Table 1 Pump Settings and Average Hemodynamic Parameters From 4 Cases

Status	Speed (rpm)	Pulsatility (%)	Beat rate (bpm)	Left flow (liter/min)	Right flow (liter/min)	LAP (mm Hg)	RAP (mm Hg)	Atrial delta P (mm Hg)	AoP (mm Hg)	PAP (mm Hg)	SVR/PVR	Pump power (W)
Baseline	3,500	15	80	2.3	2.5	4.2	8.0	−3.8	60.7	25.1	2.5	2.7
1) Change speed	3,000	15	80	2.1	1.5	7.5	7.1	0.4	63.4	22.1	2.2	2.0
	4,000			3.2	3.3	3.0	4.7	−1.6	87.8	29.3	3.0	4.1
	4,500			3.5	3.7	2.5	2.6	−0.1	108.3	31.8	3.7	5.5
	5,000			3.4	3.0	1.9	−2.0	4.0	114.9	38.5	3.6	6.3
2) Change beat rate	3,500	15	80	2.1	2.1	6.5	7.1	−0.6	65.7	24.5	3.2	2.4
			100	2.2	2.4	4.7	7.5	−2.8	63.3	25.0	2.6	2.4
			120	2.2	2.4	3.7	6.9	−3.2	62.4	24.6	2.6	2.4
3) Change pulsatility	3,500	0	80	2.4	2.7	1.9	7.3	−5.4	59.2	25.3	1.9	2.5
		10		2.2	2.5	4.2	7.7	−3.6	61.9	24.8	2.7	2.5
		15		2.2	2.5	3.4	6.6	−3.1	61.6	24.2	3.4	2.5
		25		2.6	2.5	5.0	7.1	−2.1	61.5	24.6	4.8	2.7
4) High SVR	3,500	15	80	1.6	0.8	23.8	7.4	16.4	65.1	27.9	12.4	2.2
5) High PVR				1.3	0.5	−4.9	12.9	−17.8	32.8	45.0	1.0	2.0
6) High SVR + high PVR				1.0	0.2	7.5	10.6	−3.1	46.1	41.6	0.9	1.9
7) Low SVR + low PVR				3.5	2.63	−5.7	4.6	−10.3	44.7	22.6	2.3	2.7
8) High SVR + low PVR				2.2	0.69	21.7	7.7	13.9	77.6	27.6	166.4	2.4
9) Low SVR + high PVR				1.8	0.67	−14.9	11.8	−26.7	27.2	41.2	0.7	2.1
10) High volume				2.8	3.01	19.6	22.2	−2.6	70.2	33.9	4.3	2.7
11) Low volume				1.6	0.99	−10.2	−3.0	−7.3	27.2	14.8	1.3	2.1

Abbreviations: AoP, arterial pressure; LAP, left atrial pressure; PAP, pulmonary artery pressure; PVR, pulmonary vascular resistance; RAP, right atrial pressure; SVR, systemic vascular resistance.

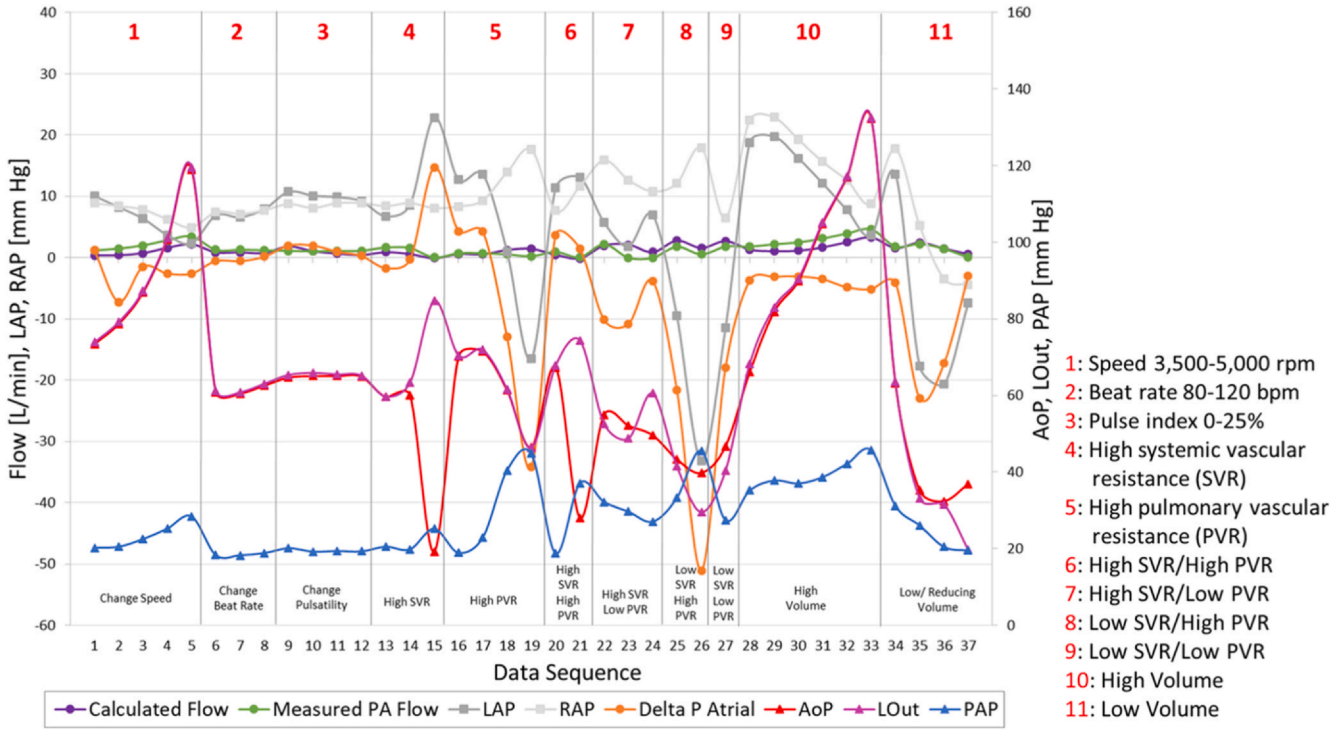

Figure 3 Time chart of the hemodynamic parameters from 1 in vivo experiment. AoP, arterial pressure; LAP, left atrial pressure; PA, pulmonary artery; PAP, pulmonary arterial pressure; RAP, right atrial pressure.

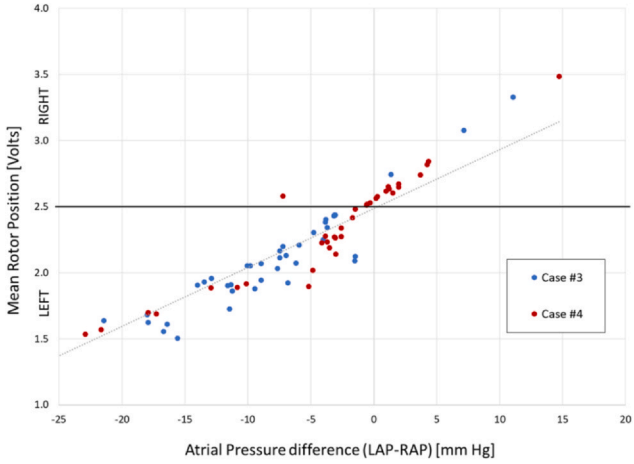

Figure 4 Plots of mean rotor position P-CFTAH per each atrial pressure difference between LA and RA in the last 2 experiments with the Hall sensors. LA, left atrium; LAP, left atrial pressure; P-CFTAH, pediatric continuous-flow total artificial heart; RA, right atrium; RAP, right atrial pressure.

pump's self-balancing feature. Additionally, under dynamic changes of various in vivo circumstances, the sensing device, as well as the pump itself, produced reasonable responses.

This study has several limitations; first, the number of animals used for HES-embedded device implantation is limited to the 2 cases. While these lambs provided valuable insights, they will never be able to fully represent key factors of small children requiring TAH implantation. Especially, CHD patients commonly have complicated and various heart anomalies that cannot be reproduced in the healthy lambs. At the onset of the study, the angle of the inlets and outlets of the P-CFTAH were to be adjustable, but over the course of a previous fitting study of this device, also performed with a 3D model with angle-adjustable inflows/outflows,[18] it has been established that the current design is the optimum, and able to accommodate most of the congenital heart anomalies. In cases of dextrocardia, or other unique clinical conditions, the pump can be implanted by flipping horizontally and/or adjusting the length of the grafts/cuffs, as guided by specific patient anatomy and device-use strategy. This, however, still needs more careful evaluation and confirmation with actual clinical cases before human implantation.

Second, the study did not involve a comprehensive biocompatibility test, including hemolysis evaluation. Assessing any potential hemolytic effects is essential when ensuring the safety and effectiveness of the P-CFTAH pump. Another limitation is the short duration of the experiment. Data collection was limited to the end of the surgery for this series and, therefore, lacks necessary long-term survival data in the postoperative phase.

Long-term studies will be necessary to acquire data surrounding the device's durability, potential complications, and overall effectiveness in supporting systemic circulation over time. Addressing these limitations in future projects will contribute to the later development of safer and more effective TAHs for critical pediatric patients.

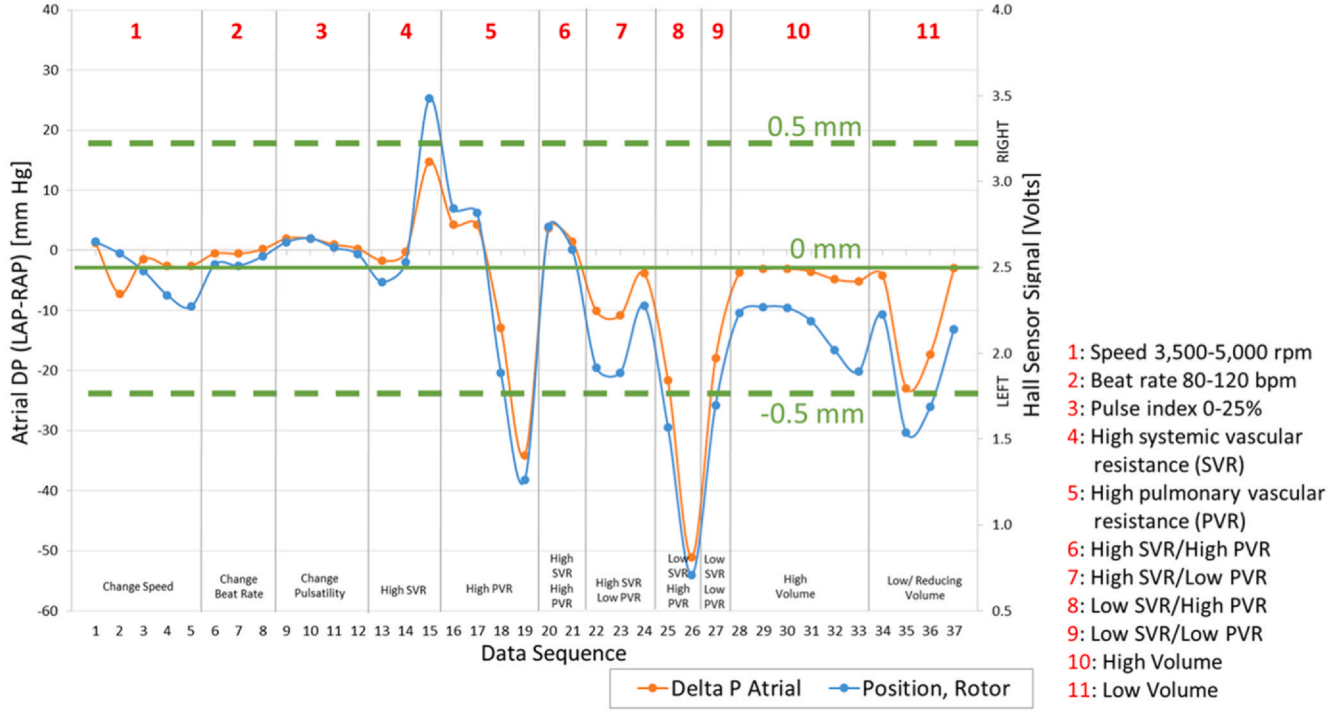

Figure 5 Time chart of changes in delta pressure (pressure difference between the atria) and rotor position, which matched throughout the case. LAP, left atrial pressure; RAP, right atrial pressure.

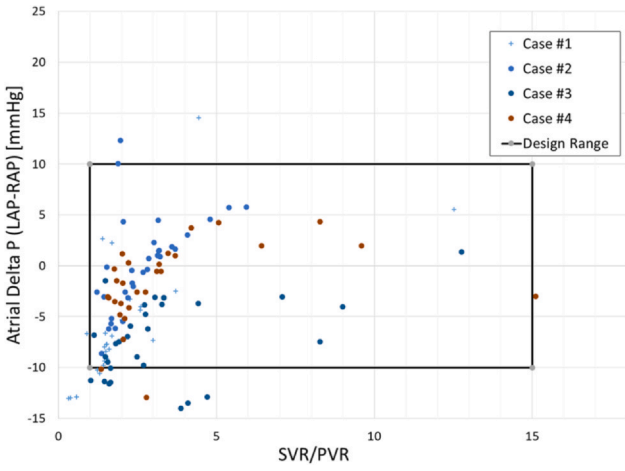

Figure 6 Plots of the atrial delta pressure in each measuring point in various systemic and pulmonary vascular resistance ratio. Design range is SVR/PVR = 1.0 to 15.0, and for 120 among 147 points, the differences between LAP and RAP remained ± 10 mm Hg. LAP, left atrial pressure; PVR, pulmonary vascular resistance; RAP, right atrial pressure; SVR, systemic vascular resistance.

Conclusion

This study evaluated the function and performance of the P-CFTAH with embedded HES in smaller-sized ovine animal models for the first time. The P-CFTAH performed within the predetermined, wide range of hemodynamic conditions and demonstrated optimal performance with the autoregulation function. HES exhibited reliable accuracy in tracking the axial movement of the rotor assembly, which allowed continuous monitoring of pump hemodynamics, independently from the pump mechanics during live support.

CRediT authorship contribution statement

All authors contributed to the design and data collection of the study. C.M., T.K., T.P., C.F., B.K., J.K., and K.F. participated in all the studies and C.M. drafted the manuscript. K.F. is the clinical principal investigator of the study. All authors critically reviewed and approved the manuscript for submission.

Disclosure statement

Jamshid H. Karimov, Barry Kuban, and Kiyotaka Fukamachi report a relationship with the National Institutes of Health that includes funding grants. There other authors declare that they have no known competing financial interests or personal relationships that could have appeared to influence the work reported in this paper.

We are thankful to the Perfusion Services of Cleveland Clinic Heart and Vascular Institute, to Patrick Grady, Jacqueline Kattar, Mary Lachowski, and Laura Konczos from the Global Cardiovascular Innovation Center, Shengqiang Gao and Jianzhong Cang of the Lerner Research Institute, and Drs Kimberly Such and George Voros, of the Biological Resources Unit, Lerner Research Institute, for their significant support, valuable help, and technical assistance with these studies.

This study was supported by funding from the National Heart, Lung, and Blood Institute, National Institutes of Health (NIH), (R01HL139984) (PI: Fukamachi).

Appendix A. Supporting information

Supplementary data associated with this article can be found in the online version at doi:10.1016/j.jhlto.2024.100118.

References

1. Singh TP, Hsich E, Cherikh WS, et al. The International Thoracic Organ Transplant Registry of the International Society for Heart and Lung Transplantation: 23rd pediatric heart transplantation report-2020; focus on deceased donor characteristics. J Heart Lung Transplant 2020;39:1028-37.
2. Singh TP, Cherikh WS, Hsich E, et al. The International Thoracic Organ Transplant Registry of the International Society for Heart and Lung Transplantation: twenty-fourth pediatric heart transplantation report - 2021; focus on recipient characteristics. J Heart Lung Transplant 2021;40:1050-9.
3. Singh TP, Cherikh WS, Hsich E, et al. The International Thoracic Organ Transplant Registry of the International Society for Heart and Lung Transplantation: twenty-fifth pediatric heart transplantation report-2022; focus on infant heart transplantation. J Heart Lung Transplant 2022;41:1357-65.
4. Conway J, Miera O, Adachi I, et al. Worldwide experience of a durable centrifugal flow pump in pediatric patients. Semin Thorac Cardiovasc Surg 2018;30:327-35.
5. Conway J, St Louis J, Morales DLS, Law S, Tjossem C, Humpl T. Delineating survival outcomes in children < 10 kg bridged to transplant or recovery with the Berlin heart EXCOR ventricular assist device. JACC Heart Fail 2015;3:70-7.
6. Kreuziger LB, Massicotte MP. Adult and pediatric mechanical circulation: a guide for the hematologist. Hematol Am Soc Hematol Educ Program 2018;2018:507-15.
7. Morales DLS, Adachi I, Peng DM, et al. Fourth annual pediatric interagency registry for mechanical circulatory support (pedimacs) report. Ann Thorac Surg 2020;110:1819-31.
8. Morales DLS, Lorts A, Rizwan R, Zafar F, Arabia FA, Villa CR. Worldwide experience with the syncardia total artificial heart in the pediatric population. ASAIO J 2017;63:518-9.
9. Rossano JW, Goldberg DJ, Fuller S, Ravishankar C, Montenegro LM, Gaynor JW. Successful use of the total artificial heart in the failing Fontan circulation. Ann Thorac Surg 2014;97:1438-40.
10. Beasley GS, Allen K, Pahl E, et al. Successful bridge to transplant in a pediatric patient using the syncardia 50 cc total artificial heart. ASAIO J 2020;66:e33-5.
11. Kirklin JK. Advances in mechanical assist devices and artificial hearts for children. Curr Opin Pediatr 2015;27:597-603.
12. Devaney EJ. The total artificial heart in pediatrics: expanding the repertoire. J Thorac Cardiovasc Surg 2016;151:e73-4.
13. Karimov JH, Horvath DJ, Byram N, et al. Early in vivo experience with the pediatric continuous-flow total artificial heart. J Heart Lung Transplant 2018;37:1029-34.
14. Horvath D, Byram N, Karimov JH, et al. Mechanism of self-regulation and in vivo performance of the Cleveland Clinic continuous-flow total artificial heart. Artif Organs 2017;41:411-7.
15. Fukamachi K, Karimov JH, Sunagawa G, et al. Generating pulsatility by pump speed modulation with continuous-flow total artificial heart in awake calves. J Artif Organs 2017;20:381-5.
16. Kobayashi M, Horvath DJ, Mielke N, et al. Progress on the design and development of the continuous-flow total artificial heart. Artif Organs 2012;36:705-13.
17. Fukamachi K, Karimov JH, Horvath DJ, et al. Initial in vitro testing of a paediatric continuous-flow total artificial heart. Interact Cardiovasc Thorac Surg 2018;26:897-901.
18. Miyagi C, Karimov JH, Kado Y, et al. Initial fitting study of a pediatric continuous-flow total artificial heart. J Heart Lung Transplant 2021;40:S174.
19. Adachi I, Peng DM, Hollander SA, et al. Sixth annual pediatric interagency registry for mechanical circulatory support (pedimacs) report: the Society of Thoracic Surgeons pedimacs annual report. Ann Thorac Surg 2023;115:1098-108.
20. Almond CS, Morales DL, Blackstone EH, et al. Berlin heart excor pediatric ventricular assist device for bridge to heart transplantation in us children. Circulation 2013;127:1702-11.
21. Bhunia SK, Kung RT. Indirect bronchial shunt flow measurements in AbioCor implantable replacement heart recipients. ASAIO J 2004;50:211-4.